

See discussions, stats, and author profiles for this publication at: <https://www.researchgate.net/publication/232659524>

Investigations into the Structure of Nitrogen-Containing CMK-3 and OCM-0.75 Carbon Replicas and the Nature of Surface Functional Groups by Spectroscopic and Sorption Techniques

ARTICLE *in* THE JOURNAL OF PHYSICAL CHEMISTRY C · JANUARY 2010

Impact Factor: 4.77 · DOI: 10.1021/jp909529x

CITATIONS

21

READS

60

3 AUTHORS:



Maria Lezanska
Nicolaus Copernicus University

27 PUBLICATIONS 202 CITATIONS

[SEE PROFILE](#)



Piotr Pietrzyk
Jagiellonian University

45 PUBLICATIONS 513 CITATIONS

[SEE PROFILE](#)



Zbigniew Sojka
Jagiellonian University

207 PUBLICATIONS 2,119 CITATIONS

[SEE PROFILE](#)

Investigations into the Structure of Nitrogen-Containing CMK-3 and OCM-0.75 Carbon Replicas and the Nature of Surface Functional Groups by Spectroscopic and Sorption Techniques

Maria Lezanska,^{*†} Piotr Pietrzyk,[‡] and Zbigniew Sojka^{‡,§}

Faculty of Chemistry, Nicolaus Copernicus University, Gagarina 7, 87-100 Toruń, Poland, Faculty of Chemistry, Jagiellonian University, Ingardena 3, 30-060 Krakow, Poland, and Regional Laboratory of Physicochemical Analyses and Structural Research, Jagiellonian University, Ingardena 3, 30-060 Krakow, Poland

Received: October 5, 2009; Revised Manuscript Received: November 9, 2009

Mesoporous silica matrixes (SBA-15) and multilamellar vesicular (MLV) structures have been used for preparation of their nitrogen-containing carbon replicas from a pyrrole precursor. The materials have been characterized with microscopic (TEM), spectroscopic (XPS, Raman, EPR), and sorption techniques. The obtained data show that the resultant CMK-3 and OCM-0.75 replicas exhibit well-developed structures of organized graphene layers, which include surface nitrogen groups located on the graphene sheets and their edges. Influence of the siliceous template loading with FeCl_3 on the microstructure of the carbons and speciation of nitrogen has been studied. The built-in nitrogen appears in various surface functional groups that have been identified and quantified with XPS. These groups play a significant role in functionalization of the carbons toward enhanced sorption capacity. The number of paramagnetic defects has been related to the preparation stage of a carbon replica as well as to the chemical status of the heteroatom. A simple model of the surface structure of the materials, based on the spectroscopic data, has been developed.

Introduction

Nitrogen-containing carbon nanomaterials of high surface area are recently receiving a great deal of attention in the literature, owing to their specific structure and unique properties.¹ For example, they exhibit an enhanced sorption capacity of anions, resulting from a positively charged carbon surface. Another important field of application of these materials as catalytic supports results from an improved thermal stability brought about by the incorporated heteroatoms.² Nitrogen-bearing carbons can be prepared via postsynthetic treatment, e.g., by heating the preoxidized samples in the stream of NH_3 or HCN .³ Ammonoxidation, a direct reaction with an ammonia–air gas mixture, supposedly proceeds at aliphatic substituents of the aromatic rings only.⁴ Ammination, in turn, consists of a reaction of ammonia with a carbon material preoxidized with HNO_3 . It is presumed to take place at carboxylic acid sites formed upon oxidation. However, N-containing functional groups developed in such a way are often unstable. To avoid this disadvantage, a suitable carbon precursor containing a controlled amount of nitrogen can be used. Easily polymerizing monomers, such as pyrrole, are the best candidates for the carbon precursors.^{5–8} Following this method, microporous carbon materials with the N content as high as 9 wt % were obtained.⁹ A different method for preparing nitrogen-containing carbon replicas, based on the chemical vapor deposition on inorganic matrixes, yields highly graphitized materials with excellent structure ordering. As reported in the literature, carbonaceous replicas containing up to 8.8 wt % of N were obtained by this method, using SBA-15, SBA-12, MCM-41, and MCM-48 templates and acetonitrile as

the carbon precursor.¹⁰ The carbon materials prepared by both methods, i.e., ammonia surface treatment and polymerization followed by pyrolysis of the pyridine precursor, show basic properties due to the presence of pyridinic nitrogen. This functionality enables catalytic removal of SO_x ¹¹ or oxidative retention of H_2S and SO_2 .¹² The carbon materials used for the SO_2 removal exhibit high water sorption capacity as well.²

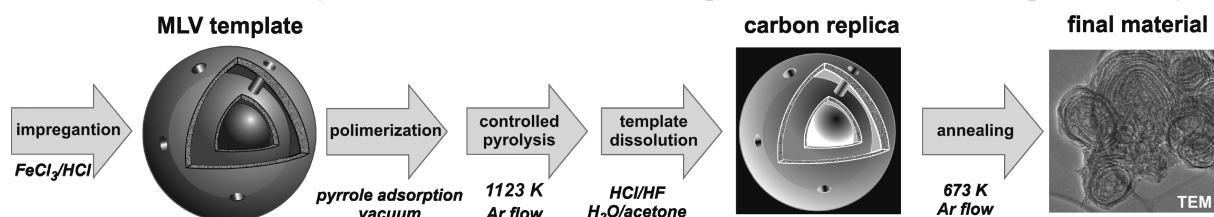
Adsorption processes occurring on carbonaceous surfaces depend on the geometry and polarizability of the adsorptive molecules. Because of the surface homogeneity, the graphitized carbon black is an ideal adsorbent for separation of isomers of similar physicochemical properties but of different geometrical structure.¹³ Introduction of chemical groups containing nitrogen on the carbon surface enhances the specific adsorption affinity of the material. As shown by the Raman and XPS results, the basic sites in such a case are mainly associated with the nitrogen-containing defects located on the basal planes of the graphene layers.⁴ Heteroatoms, like nitrogen or oxygen atoms, generate surface polarity, conventionally measured by means of water sorption or immersion calorimetry.¹⁴ It has been assumed that water molecules interact with heteroatoms constituting polar sites located at the graphene edges. The enthalpy of water sorption increases linearly with the number of such sites. The carbonaceous replicas discussed in this work were prepared via oxidative polymerization of pyrrole inside the mesopores of ordered silica matrixes loaded with FeCl_3 . To establish which factor, structure or composition of carbons containing heteroatoms, mostly influences the physicochemical properties of the materials, the newly synthesized carbonaceous replicas obtained using multilamellar vesicular (MLV) matrixes were compared with those prepared from SBA-15.⁵ On the basis of the results of combined use of sorption and spectroscopic techniques, these materials were used for establishing the nature of the nitrogen sites.

* To whom correspondence should be addressed. E-mail: miriam@chem.uni.torun.pl. Phone: +48 56 611 47 52. Fax: +48 56 654 24 77.

† Nicolaus Copernicus University.

‡ Faculty of Chemistry, Jagiellonian University.

§ Regional Laboratory of Physicochemical Analyses and Structural Research, Jagiellonian University.

SCHEME 1: Illustration of the Synthesis Procedure Utilized for Preparation of OCM Carbon Replicas from Pyrrole**TABLE 1:** Compositions and Selected Sorption Properties of the Studied Carbons

sample	S_{BET} (m ² /g)	N cont./(C/N) ^a (wt %/mol)	N cont./(C/N) ^b (wt %/mol)	O cont. ^b (wt %)	F cont. ^b (wt %)	Si cont. ^b (wt %)	Fe cont. ^b (wt %)	V_{mi}^c (cm ³ /g)	V_{mes}^c (cm ³ /g)	S_{ext}^c (cm ² /g)
CMK-3N1.25	1636	4.6/11.4	5.0/17.7	4.5	2.1	0.23	0.41	0.100	1.296	174.4
CMK-3N2.00	2021	5.0/11.8	4.4/20.5	5.3	0.5	0.20	0.41	0.123	1.640	188.4
OCM-0.75N0.25	1083	6.6/11.4	6.2/13.9	6.9	0.7	0.43	0.50	0.050	0.828	35.0
OCM-0.75N0.75	797	6.4/11.9	6.5/13.2	6.6	1.6	0.11	0.36	0.072	0.474	30.2
OCM-0.75N1.25	1031	6.5/11.9	6.2/13.9	5.7	1.5	0.11	0.63	0.070	0.317	546.8
OCM-0.75N2.00	1347	5.9/11.4	10.6/7.3	10.9	0.0	0.75	0.88	0.064	1.088	433.6

^a The samples are not entirely burnt under elemental analysis conditions; thus, the results of the elemental analysis are only estimates of the contents of C, H, and N (the total content of C, H, and N does not exceed 85%); ^b XPS analysis confirms that the whole silica and Fe species have not been removed. ^c V_{mi} , V_{mes} , and S_{ext} were obtained from the α_s plots. More detailed characterization of the sorption properties can be found elsewhere.⁸

Materials and Methods

The siliceous materials were synthesized hydrothermally according to a standard procedure.¹⁵ The SBA-15 and MLV-0.75 templates were obtained using the following molar gel composition: 1 TEOS: 6 HCl: 196 H₂O: 1.72×10^{-2} P123. In addition, 2.08×10^{-4} mol of 1,3,5-TMB per 1 mol of TEOS was added to the reaction mixture during the synthesis of the MLV-0.75 material. All of the mixtures were autoclaved at 373 K for 24 h. The obtained samples were heated at 773 K for 4 h under nitrogen and then calcined at 783 K for 5 h in air. The carbon replicas were prepared via oxidative polymerization of pyrrole during a stoichiometric reaction with ferric chloride that was introduced into the mesopores of the inorganic template (Scheme 1).⁵ The pyrrole infiltration was performed under a vacuum, and the process was repeated with a new portion of pyrrole. The carbonization temperature was 1123 K. The carbon–silica composites were then thoroughly washed, subsequently with a 40% HF–acetone mixture, concentrated HCl, and deionized water, to remove the inorganic template. The obtained samples are designated as CMK-3Nx (replicas of SBA-15) and OCM-0.75Nx (replicas of MLV-0.75), where x denotes the amount of FeCl₃ in grams (0.25, 0.75, 1.25, and 2.00) per 1 g of the siliceous template. The OCM acronym stands for an onion-like carbonaceous material.

The TEM (transmission electron microscopy) images of the carbonaceous replicas were obtained with a Hitachi HF 2000 microscope (200 kV). Prior to the analysis, the samples were dusted on a copper Lasey grid. The TEM analysis was combined with the EDX (energy-dispersive X-ray) spectroscopy measurements. The BET (Brunauer–Emmett–Teller) specific surface area (S_{BET}) was determined by the α_s -plot method, using nongraphitized carbon black as a reference. Adsorption isotherm data over the relative pressure (p/p_s) range 0.05–0.15 were utilized in the α_s -plot analysis. The isotherms of the nitrogen sorption were recorded with an automated volumetric analyzer (ASAP 2010, Micromeritics) at 77 K. The adsorption of water vapor was measured at 298.2 K, using a homemade vacuum device equipped with quartz-spring McBain balances and MKS Baratron gauges. The TG (thermogravimetry) measurements for carbons were performed using a TA Instruments SDT 2960 analyzer. The TG data were recorded up to 850 °C (2 °C/min)

in flowing air. The XPS (X-ray photoelectron spectroscopy) analyses were carried out with a MICROLAB-350 spectrometer using the Al K α radiation. The spectra were fitted with use of the XPSPEAK4.1 software. The standard Shirley method for both background subtraction and spectrum deconvolution was applied, assuming a mixed Gaussian–Lorentzian (25–30%) line shape. The energy correction, based on the C 1s peak position at 284.5 eV, was made to account for sample charging. Self-supporting pellets containing 10 mg of the studied material and 90 mg of KBr were used for the microRaman measurements. The spectra were recorded at room temperature, using a Renishaw InVia spectrometer with a resolution of 2 cm⁻¹, equipped with a Leica DMLM confocal microscope and a CCD detector. An excitation wavelength of 514.5 nm was provided by an Ar-ion laser (Spectra-Physics, model 2025). The laser power at the sample position was about 5 mW. The Raman scattered light was collected in the spectral range 100–3200 cm⁻¹. Eight scans were accumulated to ensure a sufficient signal-to-noise ratio. The EPR (electron paramagnetic resonance) measurements were performed with a Bruker ELEXSYS E500 spectrometer operating at the X-band and 100 kHz modulation. The spectra were recorded at the liquid nitrogen temperature with a modulation amplitude of 3 G and microwave power of 1–10 mW. VOSO₄·5H₂O diluted in a diamagnetic K₂SO₄ host containing 5×10^{19} spins/g was used as a primary standard for quantitative measurements.¹⁶

Results and Discussion

Composition and Textural Characterization. Two series of mesoporous carbon replicas (CMK-3 and OCM-0.75) were examined in order to characterize nitrogen species present in these materials. The chemical composition of the studied materials is summarized in Table 1. The analysis reveals that they still preserve some Si residues and contain up to 0.9 wt % of iron used in the synthesis. Nitrogen and oxygen atoms of the functional groups constitute 4.4–10.6 and 4.5–10.9 wt %, respectively. The type of the applied matrix does not directly influence the amount of nitrogen built in the replica structure. The OCM-0.75Nx samples contain slightly more nitrogen as compared to the CMK-3Nx ones (6.5 and 4.6 wt % as well as 5.8 and 5.0 wt %, respectively). Moreover, the amount of the

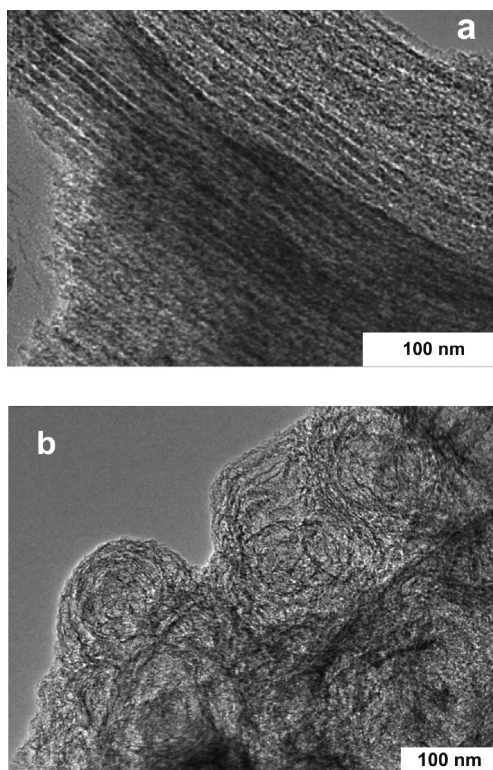


Figure 1. TEM images of CMK-3N2.00 (a) and OCM-0.75N1.25 (b).

incorporated nitrogen apparently does not correlate with the amount of FeCl_3 but seems to influence strongly the speciation of nitrogen (see below). As known, FeCl_3 not only plays the role of a polymerization catalyst, but it also promotes pyrrole graphitization during carbonization.¹⁷

The results of the present study confirm that the contents of nitrogen in the examined carbons (Table 1) constitute only ca. 1/3 of the N amount present in polypyrrole (PPy) subjected to carbonization. During the latter process, nitrogen is partially being removed in the form of HCN, N_2 , or NH_3 from the carbon structure, which leads to reduction in the N/C ratio of the material.¹⁸ The GC-MS and FTIR analyses of products of the PPy degradation, performed during carbonization of the PPy/PET fibers, indicated that denitrogenation occurs mostly at temperatures above 600 °C (with a maximum of the HCN evolution at 637 °C), i.e., when less thermally stable PET had been removed (at 400 °C). The two analytical methods did not reveal products of the decomposition of the pyrrole monomer or oligomers as fragments of the PPy backbone. These results prove the high thermal stability of PPy.¹⁹ In the case of doped (FeCl_3) PPy nanoparticles, the loss of nitrogen in the form of the above-mentioned compounds occurs between 400 and 600 °C and the carbonization reactions produce polycondensed aromatic hydrocarbons.¹⁷

The degradation of PPy occurs in the presented carbonaceous materials presumably in a similar way, although it is possible that a slight PPy fraction starts to degrade already at 90 °C in the presence of traces of air contained in the sample that is then subjected to carbonization under an argon atmosphere. The evolution of NH_4Cl , CO_2 , and CO implies opening of the pyrrole rings during heating of PPy at 90 °C in air.²⁰ All of the studied replicas show a well-developed surface (Table 1). The CMK-3Nx materials, being replicas of SBA-15, exhibit a well-ordered structure. Figure 1a shows a typical TEM image of the CMK-3N2.00 sample. An ordered microstructure of the material with a hexagonal arrangement of carbon rods is clearly seen. A larger

amount of the applied FeCl_3 led to a greater average thickness of the matrix walls and a smaller effective diameter of the mesopores. Thus, the prepared replicas exhibit narrower walls and a larger average pore diameter. As a consequence, Fe-modified SBA-15 of a lower sorption capacity gives a replica with a higher sorption capacity, in accordance with the S_{BET} measurements (Table 1). A peak at ca. 4.2 nm, associated with cavitation,⁸ appears in the BJH (Barrett–Joiner–Halenda) pore size distribution curves for the studied materials. We suggest that ink bottle-like pores (i.e., pores with narrower entrances) are present in all of the OCM samples. The mentioned peak indicates that diameters of these pores are above 5–6 nm and the entrance window diameters are below 4.0 nm. Because OCMs exhibit a nontypical pore structure, their pore size cannot reliably be determined by the BJH method, including the assumption that pores are cylindrical. On the basis of the TEM image of the best-ordered sample (OCM-1.25N), the diameters of spherical pores located between carbonaceous walls have been estimated to be 6–9 nm (Figure 1b).

The replicas of MLV-0.75 exhibit inferior structure ordering in comparison to those of CMK-3Nx (Figure 1). In the low-angle XRD patterns of OCM-0.75Nx (results not shown), diffraction lines were virtually absent, implying that those materials were basically amorphous. The morphology of OCM-0.75Nx significantly varies, depending on the amount of FeCl_3 used in the synthesis. In general, with the increasing amount of the applied oxidant, differently shaped materials of foam-, onion-, sheath-, and sheath-onion-like structures are formed, respectively.⁸

The OCM-0.75N1.25 sample is the most homogeneous one, and it consists of regular onion-like structures only, as revealed by the TEM images (Figure 1b). The largest surface area and pore volume among all of the examined samples is observed for OCM-0.75N2.00, which exhibits a foam-like structure. The BET surface areas of the materials with the predominant onion-like structure (OCM-0.75N1.25 and OCM-0.75N0.25) are similar to each other. However, the OCM-0.75N0.75 sample exhibits the smallest surface area. This can be associated with its particular hollow onion-like structure. More detailed sorption characterization of the samples can be found elsewhere.⁸

The amounts of disordered and graphitic carbon domains in the samples were estimated from the TGA/DTA (thermogravimetric analysis/differential thermal analysis) measurements. While heating a sample in air at the 2°/min rate, two peaks were observed, low-temperature (400 °C) and high-temperature (650 °C) ones. These weight-loss steps can be assigned to distorted and ideal graphitic phases, respectively.⁶ For example, the graphite content of the CMK-3N1.25 sample was found to be ca. 4 wt %, being similar to that reported for other mesoporous carbons.⁶ It agrees well with the Raman data, indicating that the amount of pristine graphitic domains does not exceed 8 wt % (see below).

Sorption Properties. Incorporation of the nitrogen heteroatoms into the OCM-0.75 and CMK-3 structures gives rise to the formation of surface N-species revealed by the XPS analysis (vide infra), which can be probed by sorption of water (Figure 2). The mostly hydrophilic samples (OCM-0.75N1.25 and CMK-3N1.25) contain the highest concentration of N-6 and N-Q sites in total (up to 33 and 32 at. %, respectively). As a consequence, these materials exhibit high polarity, being well reflected in the results of sorption measurements (Figure 2). In particular, for the nitrogen-containing OCM carbons (Figure 2b), an increased sorption of water in comparison to earlier literature data² was observed, reaching the value $m_{\text{H}_2\text{O}} = 13 \text{ mmol/g}$ at $p/p_0 = 0.2$ in the case of OCM-0.75N1.25.

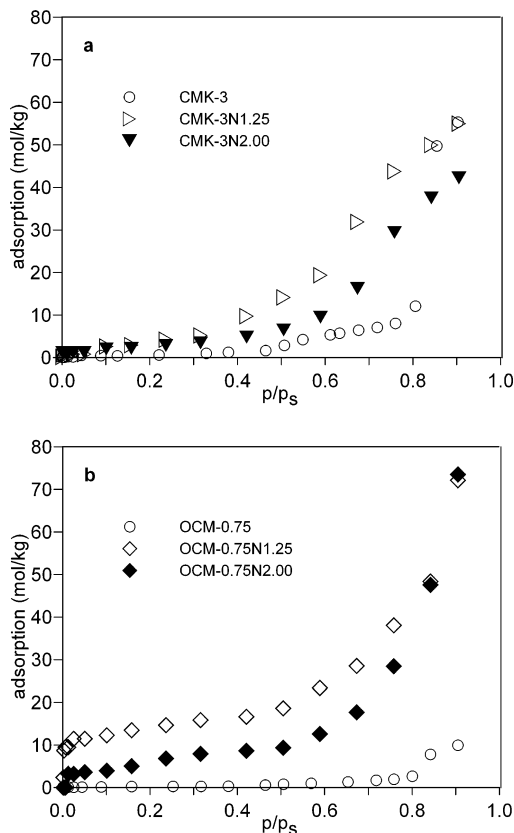


Figure 2. Isotherms of water adsorption for carbons containing nitrogen (triangles and diamonds) and carbons with no nitrogen (circles): (a) CMK-3 replicas; (b) OCM-0.75 replicas.

As compared to the CMK-3 replicas, the surface of the N-containing OCM-0.75 materials is distinctly more hydrophilic. However, it can be traced back not only to the speciation of nitrogen but also to the structure of the replicas as well. For the same value of x , the total water sorption for the OCM-N x materials is higher than that for CMK-3N x . It is consistent with the higher amount of N-6, N-X, and N-Q species in comparison to N-5 species (see XPS data), although the differences are small.

XPS C 1s Data. The core-level XPS spectra of the N-containing carbon materials exhibit six C 1s sub-bands (Figure 3), indicating the carbon atoms present in a relatively large variety of chemical states. The predominant C 1s band, centered at 284.5 eV, corresponds to the C=C (sp^2) and C—C (sp^3) carbons of graphitic and disordered graphitic species, respectively. On the basis of the literature data,^{21,22} the successive sub-bands in the long tail can be assigned to various groups including a carbon atom associated with O, N, or F, such as C—N and C—OH (285.34–286.17 eV), carbonyl and quinone groups (286.94–287.81 eV), carboxyl (288.66–289.56 eV), and possibly carbamate (289.7 eV) and a more electronegative fluorine atom (above 292.7 eV). The similar ratios of the N 1s/C 1s and O 1s/C 1s peak intensities, observed for all but the OCM-0.75N2.00 samples, are consistent with the comparable N and O contents in those samples (see Table 1).

XPS N 1s Data. The N 1s XPS spectra of the examined carbon replicas are shown in Figure 4, whereas the binding energies are listed in Table 2. Four different peaks centered at 398.6 ± 0.3 (N-6), 400.5 ± 0.3 (N-5), and 401.3 ± 0.3 (N-Q) as well as a peak at 402–405 eV (N-X) were delineated by the curve fitting of the spectra of CMK-3N x and OCM-0.75N x . During pyrolysis, various functionalities, such as pyridines, protonated pyridinic nitrogen, and its N-oxide derivatives, are

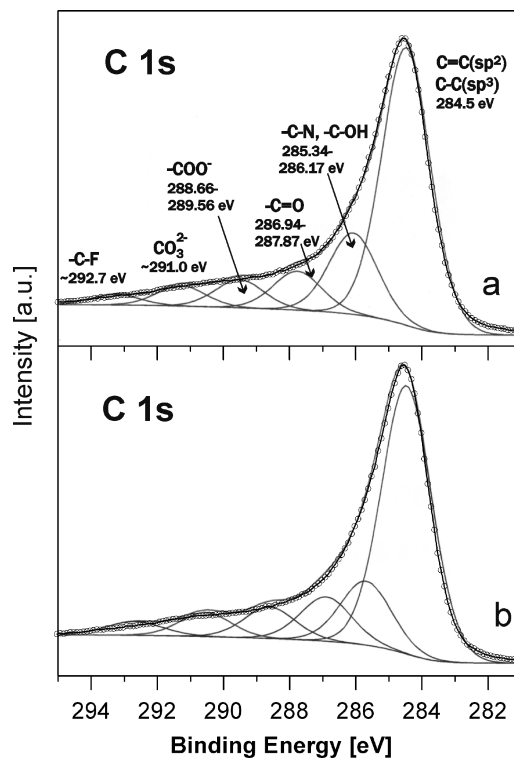


Figure 3. Exemplary XPS C 1s spectra of OCM-0.75N1.25 (a) and OCM-0.75N2.00 (b).

formed from the polypyrrole fragments.²³ According to the literature, the N-6 band is assigned to the pyridine nitrogen, the only nitrogen-bearing species suggested to survive at 1223 K.² The N-5 nitrogen is assigned to the 5-membered ring entities corresponding to the pyrrolic and/or pyridone nitrogen. The pyrrolic group is stable up to 873 K, and above this temperature, it converts into N-6 and N-Q.² During carbonization, PPy transforms into 6-membered rings, being the most stable chemical structure. Cyclization, hydride ion transfer, and condensation accompanied by partial removal of nitrogen are primary reactions occurring during the carbonization process. Thus, it is rather unlikely that the peak at 400.5 eV originates from the pyrrolic groups. Probably, it refers to the pyridone groups (as shown in Figure 4). Several possible structures can be associated with the N-Q band that is not stable at 1123 K. In general, the binding energy of ca. 401.5 eV represents a classic quaternary nitrogen structure, like that of the ammonium ion, but no such functionality in carbons is evidenced. However, the existence of protonated pyridinic N, depending on the acidity of carbon material, cannot be excluded but is hardly probable in this case. The N-Q nitrogen atoms are supposed to replace the carbon atoms in the graphene sheets and can be located at a “center” or “valley” position.²³ The diagnostic binding energies at 401.3 ± 0.1 eV for the valley and center N atoms have been established, based on previously published XPS spectra of chars.²³ The N-X line corresponds to a pyridine N-oxide, which was produced by postpyrolysis oxidation upon exposure of the samples to ambient conditions.

Above 723 K, a part of the pyridinic N-6 groups transforms into the N-Q species, but above 873 K, the N-6/N-Q ratio does not vary anymore. Thus, all of the nitrogen atoms incorporated into the synthesized carbon materials are eventually associated with the 6-membered rings located at the graphene edges (pyridinic N) or in the interior of the graphene sheets (quaternary N). Inspection of the quantitative data summarized in Table 2 shows for the CMK samples that nitrogen is preferentially

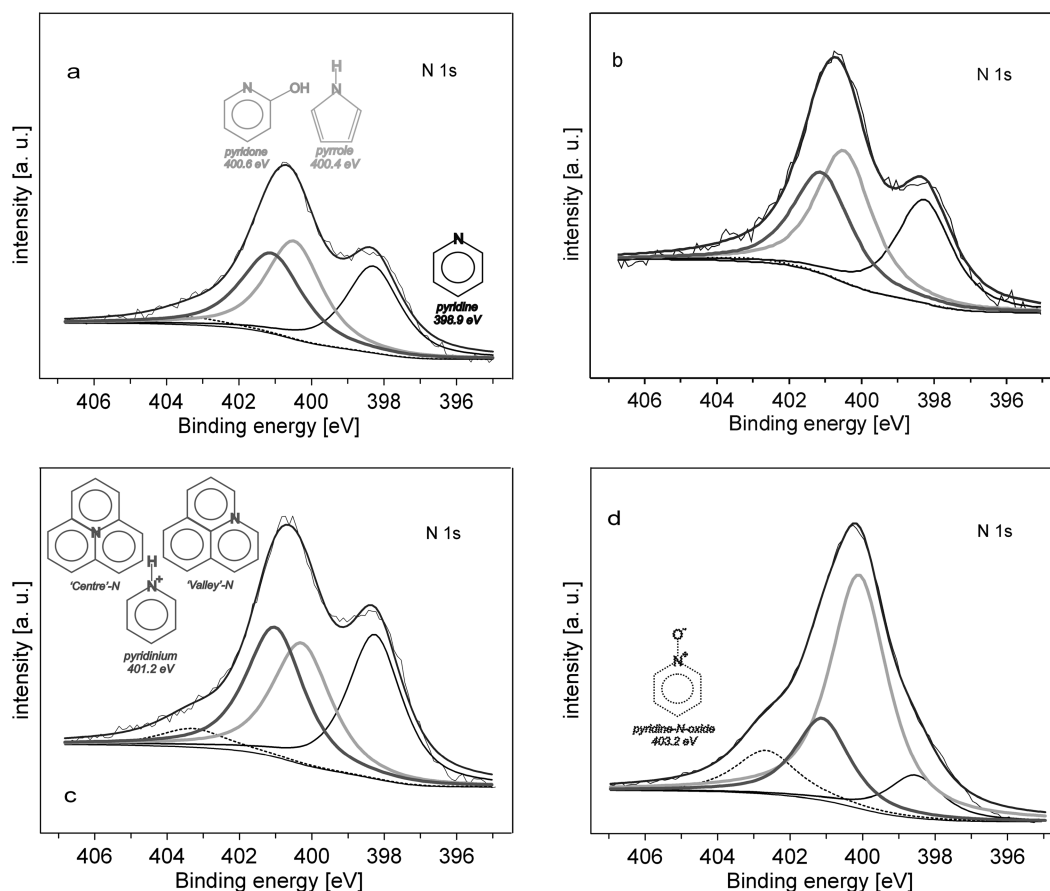


Figure 4. Deconvolution of XPS N 1s spectra of CMK-3N1.25 (a), CMK-3N2.00 (b), OCM-0.75N1.25 (c), and OCM-0.75N2.00 (d). The individual bands correspond to the depicted molecular structures.

TABLE 2: Binding Energies of Particular N Atoms and Their Contributions (at. %) in Total N Obtained from Fitting of the N 1s XPS Spectra

sample	N-pyridine (N-6) (~398.5 eV)		N-pyrrole/N-pyridone (N-5) (~400.5 eV)		N-“valley”, N-“center” (N-Q) (~401.2 eV)		pyridine-N-oxide (N-X) (~403.2 eV)	
	BE (eV)	at. %	BE (eV)	at. %	BE (eV)	at. %	BE (eV)	at. %
CMK-3N1.25	398.30	30.43	400.48	34.80	401.10	31.61	403.30	3.16
CMK-3N2.00	398.27	30.13	400.48	38.08	401.10	30.53	403.30	1.25
OCM-0.75N0.25	398.30	33.28	400.29	48.07	401.09	14.94	402.80	3.71
OCM-0.75N0.75	398.26	35.56	400.38	51.83	401.38	10.00	403.39	2.60
OCM-0.75N1.25	398.26	33.35	400.28	29.91	401.02	31.49	403.40	5.26
OCM-0.75N2.00	398.55	10.17	400.10	58.71	401.11	19.53	402.67	11.59

localized at the edges, whereas, in the case of the OCM materials, the distribution between the outer and inner sites is more even.

In the case of the smallest quantities of FeCl_3 , used during the preparation of the OCM-0.75N0.25 and OCM-0.75N0.75 materials, the carbon agglomerates contain the smallest amounts of the N-Q-type nitrogen (14.94 and 10.00 at. %, respectively), located in the interior of the graphene structures (Table 2). Consequently, the highest content of the N-Q nitrogen was found for CMK-3N1.25 and OCM-0.75N1.25, containing mainly aromatic carbons (vide Raman data), which were synthesized at relatively high FeCl_3 loadings. In the case of the OCM-0.75N2.00 sample, the N-Q and N-pyridinic nitrogen atoms constitute a relatively small fraction of the total nitrogen content, equal to 10.6 wt %. The presence of a large amount of oxygen (ca. 11 wt %) in this sample can be the reason for that. Oxygen atoms, occupying positions adjacent to nitrogen, give rise to the formation of the pyridone groups (N-5), dominating in this sample (58.71 at. %). A similar situation is observed for the OCM-0.75N0.25 and OCM-0.75N0.75 samples.

At elevated carbonization temperatures (1123 K), substantial portions of oxygen and nitrogen were released, creating surface defects, partly revealed by the EPR spectroscopy (vide infra). They can act as active sites for oxygen adsorption, when the carbon samples are exposed to air.²⁴ The actual oxygen content in these samples (Table 1) can be connected with this effect.

In summary, all of the XPS results (C 1s, N 1s, and O 1s) confirm that various combinations of the carbon atoms with the nitrogen and oxygen ones are present on the surface of the carbonaceous materials. For example, the peak at 285.4 eV (C 1s) may be associated with the sp^2 C–N bond in aromatic structures,²⁵ whereas C-, N-, and O-containing species, such as N-top, pyridone groups, and N-oxide (detected at 398.5, 400.5, and 403.2 eV, respectively) are formed as well (Table 2). The most highly graphitized samples (compare the Raman section) contain the largest amounts of pyridinic and quaternary nitrogen.

Raman Spectroscopy. For probing disordered carbon materials, Raman spectroscopy is a powerful technique due to its sensitivity not only toward the extended crystalline structures but also toward smaller entities with short-range order and

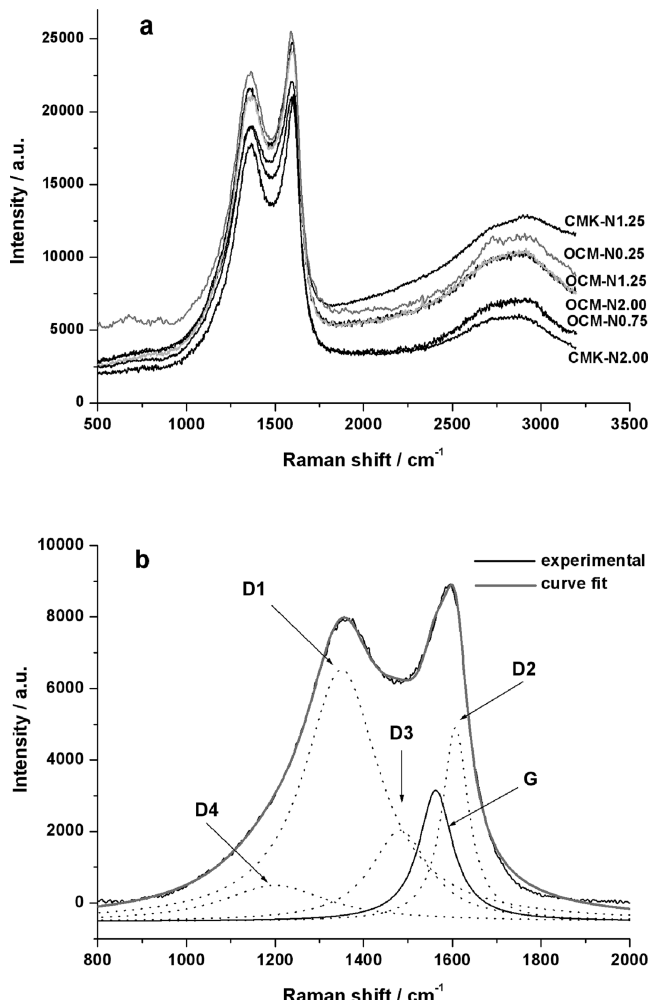


Figure 5. Raman spectra of the investigated carbon replicas (a) and results of a fitting procedure for the CMK-3N2.00 sample (b).

molecular structures. It has been used to investigate the phase composition of carbon materials like soot or different types of graphite.^{26,27}

The Raman spectra of the investigated carbon replicas are shown in Figure 5a. In all cases, two intense complex bands located at 1350 and 1580 cm^{-1} dominate. They are associated with the vibrational modes of disordered/amorphous and pristine graphene sheets, respectively. However, due to the complex nature of the spectra, their proper interpretation required a numerical decomposition into individual components. This was carried out with the GRAMS/32 software. The fit quality, gauged by the reduced χ^2 value, varied between 1 and 3, and an example of the fitting is depicted in Figure 5b. Five component signals at 1350 cm^{-1} (D1), 1612 cm^{-1} (D2), 1510 cm^{-1} (D3), 1210 cm^{-1} (D4), and 1575 cm^{-1} (G) assigned to graphene edges, graphene sheets, amorphous carbon, polyenes, and graphitic carbon, respectively, are clearly revealed in the figure.

The normalized integral intensities of the individual components, obtained from the fitting, were found to vary with the nature of the sample, i.e., with the amount of the iron precursor used and the type of the siliceous template. The most intense signal due to the disordered graphene sheets corresponds well with the dominant sp^2/sp^3 C 1s XPS peak. The disorder of the graphene sheets is caused by abundant edges and the presence of heteroatoms in the investigated materials (Figure 6).

For the CMK replicas, the intensity of the D1 band is the lowest, which agrees with the smallest content of nitrogen in

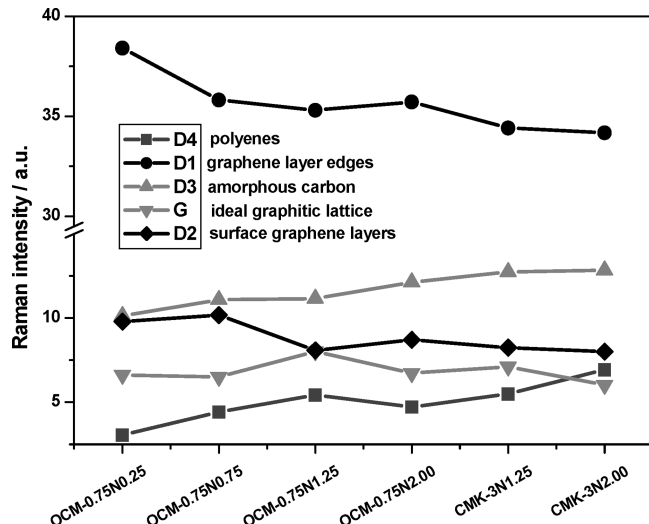


Figure 6. Normalized intensities of the D4, D1, D3, G, and D2 bands obtained by fitting the Raman spectra of the carbon replicas.

their structure (Table 1). At the same time, the amount of amorphous carbon, calculated from the band intensity ratio $I_{\text{D3}}/I_{\text{G}}$, was found to be the largest for CMK and the smallest for the OCM replicas with the iron content below 2 g of FeCl_3 per 1 g of silica (Figure 6).

It has been proposed that the parameter $I_{\text{D1}}/I_{(\text{G+D1+D2})}$ can be used to gauge the degree of graphitization of carbonaceous materials.^{26,28} Substitution of the numerical values shows that the best-organized structures are those of OCM-0.75N (0.75 and 1.25) together with CMK-3N1.25, while the smallest fraction of graphene components was found for the CMK-3N2.00 material. For all of the samples except for CMK-3N2.00, the D4 band exhibits the lowest Raman intensity, which reflects the presence of noncarbonized polyenes or impurities related to the pyrrole precursor.²⁶ The Raman data indicate that the walls of the synthesized materials are composed of scale-like graphene layers (overlapping graphene layers exhibiting a structure resembling scales; compare to the model developed in the last section) with a relatively large amount of the incorporated nitrogen. The growth of the carbon replica walls clearly depends on the siliceous template type, being favored by the OCM-type structure. The amount of the iron catalyst introduced into the templates influences also the domain composition. The best-organized graphitic domains were obtained for the moderate catalyst loadings (1.25 and 0.75 g of FeCl_3 per 1 g of the template).

The full width at half-maximum (FWHM) of the C 1s band varies with the increasing FeCl_3 content (Figure 6) in a similar way as the $I_{\text{D1}}/I_{(\text{G+D1+D2})}$ (or $I_{\text{D1}}/I_{\text{G}}$) ratio does. Usually, it is connected with the carbonization temperature.²⁹ The data presented in Figure 7 confirm that the carbon replicas prepared with 1.25 g of FeCl_3 per 1 g of the silica template exhibit the largest content of aromatic fragments. Presumably, an optimum Fe concentration exists for the most efficient pyrrole polymerization, leading to aromatic-rich (high content of the graphene layers) carbonaceous materials.

For all of the samples, the Raman spectra recorded with $\lambda_0 = 514 \text{ nm}$ exhibit second-order broad signals in the range 2300–3200 cm^{-1} (Figure 5a). The bands appearing in this region can be attributed to overtones and to the combinations of vibration modes of the graphitic layers. According to the literature,³⁰ those band positions are assigned to the 2×D4 overtone (2450 cm^{-1}), 2×D1 overtone (2700 cm^{-1}), combina-

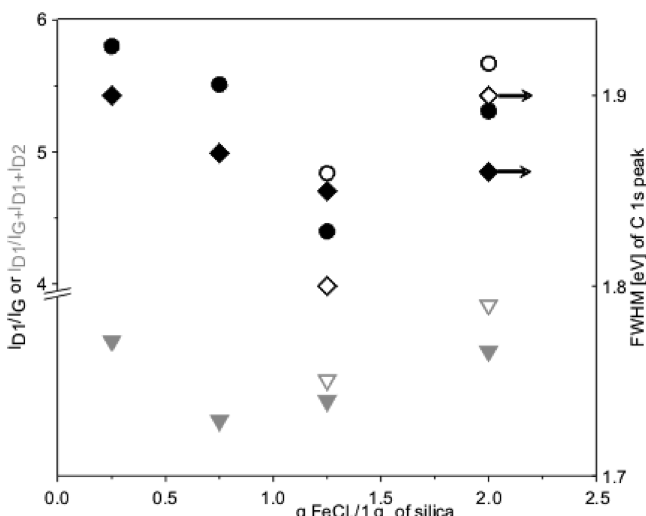


Figure 7. Changes in graphitization level, calculated from the Raman band intensities (open circles for CMK, filled circles for OCM), and FWHM for the C 1s XPS bands (diamonds) with respect to FeCl_3 loading. In gray, the ratio of the Raman intensities calculated as $I_{\text{D}1}/(I_{\text{G}} + I_{\text{D}1} + I_{\text{D}2})$.

tion band G+D1 (2900 cm^{-1}), and $2\times$ D2 overtone (3100 cm^{-1}). Their appearance confirms relatively well-organized carbon structures.

EPR Spectroscopy. All of the EPR spectra of the investigated replicas revealed a typical signal at g_{eff} around 2.0, being characteristic of carbon-related radicals. Additionally, a resonance at $g_{\text{eff}} = 4.3$, assigned to the iron(III) catalyst nonconsumed during the pyrrole polymerization, was observed. The latter was efficiently removed during dissolution and washing steps, leading to disappearance of the Fe(III) signal. Surprisingly, in the case of the CMK-3N2.00 samples, the signal due to the carbon radicals was not detected.

In principle, magnetic susceptibility of conducting carbon-related materials can be accounted for by the Curie (localized spins) and Pauli (conduction electrons, being temperature independent) contributions. At low temperatures, the EPR data show a Curie-like behavior due to the localized spins attributed to carbon dangling bonds, with a concentration of about 10^{18} spins per gram.³¹ Quantum chemical calculations show that their nature can be connected with the nonbonding paramagnetic π -electron states localized at the graphene layer edges.³² This effect is responsible for the localized states near the Fermi level. The interaction between the localized and conduction electrons leads to a relatively strong exchange narrowing. As a result, the final EPR line assumes a symmetric Lorentzian shape, which is characteristic of the extended conjugated sp^2 carbon sheets, shown in the XPS and Raman spectra.

Computer simulation of the spectra, carried out with the EPRsim32 software,³³ revealed that, for the final carbon replicas, the shape of a single EPR line at $g = 2.0055$ (Figure 8) can only be reproduced while assuming superposition of two types of paramagnetic centers of approximately the same abundance. The Gaussian component is characterized by a narrow line of the width $\Delta B_{\text{pp}} = 4.7 \text{ G}$, whereas the broad signal with $\Delta B_{\text{pp}} = 9.8 \text{ G}$ exhibits the Lorentzian shape. According to the literature, the Gaussian signal is attributed to paramagnetic centers located in fragments consisting of a few aromatic rings that form a polyene structure³⁴ revealed by the Raman spectroscopy (the D4 band, see above). The Lorentzian signal is assigned to localized spins in disordered graphene layers or graphitic-like domains, also indicated by the Raman spectra (D1 and D2

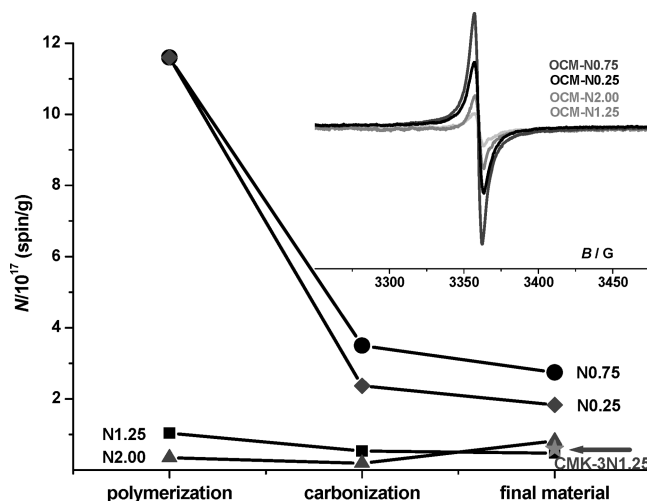


Figure 8. Changes in the number of spins for the investigated OCM-0.75 carbon replicas, related to the preparation steps (in the inset, EPR spectra for the final OCM-0.75 replicas). The arrow indicates a single experimental point (depicted with a star) for the CMK-3N1.25 sample.

bands). Extensive broadening of the Lorentzian line could be connected with the interaction of radical centers with molecular dioxygen.³⁵ The observed g values are typical of disordered carbon structures with a significant sp^3 character arising from the nonplanar part of the carbon sheets.³⁶ Also, the presence of heteroatoms can be responsible for the shift in the g value. The dipole–dipole interactions and the unresolved hyperfine structure in the case of N-bearing centers result in relatively high values of the linewidths.

Although the chemical analysis indicated a substantial amount of nitrogen (up to 6.6 wt %) incorporated into the synthesized carbon replicas, there is no resolved hyperfine splitting due to the ^{14}N nuclei ($I = 1$) in the EPR spectra. It indicates that paramagnetism in the N-containing carbon species is caused by local magnetic moments produced by carbon dangling bonds rather than due to localization of an excess electron around the N-site. The same effect was observed earlier for fluorinated graphite.³⁷ Generation of the dangling bonds with the localized spins results from the substitution of carbon atoms with nitrogen, which converts locally the sp^2 hybridization of graphite into the sp^3 one, at the expense of the π -bonds.³⁶

The EPR measurements were carried out for the samples at each of the preparation stages, i.e., polymerization, carbonization, and for final materials (Figure 8). In the case of small iron catalyst addition (N0.25 and N0.75), pyrrole polymerization leads to the formation of abundant radicals, the quantity of which is of almost 1 order of magnitude greater than that for the N1.25 and N2.00 samples. For lower catalyst loadings, it seems that the disordered structures similar in nature to polypyrrole and exhibiting a mesoscopic disorder prevail.³⁸ This situation leads to the chemical instability of the polypyrrole domains that in the course of further annealing grow together and undergo structural ordering, leading eventually to partial graphitization revealed by the Raman spectra. On the contrary, for larger catalyst contents, the number of radicals remains constant regardless of the preparation stage.

Functional Model of N-Containing Carbons. The present study suggests that large quantities of both pyridinic and quaternary nitrogen are present in the sample prepared with an optimum amount of FeCl_3 . In onion-like samples, prepared using relatively small amounts of the catalyst, larger quantities of oxygen and nitrogen (mostly the center and valley N-Q species)

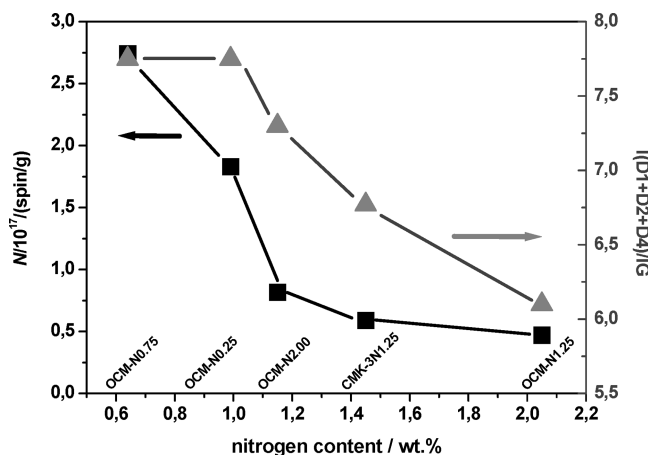
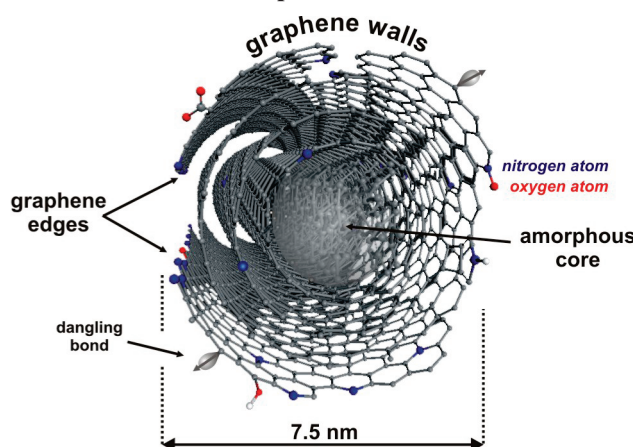


Figure 9. Influence of the nitrogen content (as calculated from XPS spectra) on the number of radicals (squares) and degree of graphitization (triangles).

SCHEME 2: Schematic Representation of an Idealized Model of a CMK-3 Rod Decorated with the Nitrogen Surface Functional Groups



are removed. Pyridinic (N-6) nitrogen seems to be more stable and resistant to removal during carbonization. On the other hand, when the amount of FeCl_3 used is relatively large (OCM-N2.00), a fraction of the pyridinic N transforms into the pyridone groups upon oxygen adsorption on defects. For CMK-3N2.00, this process is negligible.

For the final materials, it is observed (Figure 9) that the EPR signal intensity is inversely proportional to the nitrogen content (a fraction of the valley and center N), indicating that the excess electron brought by nitrogen incorporated into the carbon sheets annihilates carbon radicals. A similar effect was observed for carbon nitride films.³⁹ From the Raman data, one can conclude that the $I_{(D1+D2+D4)}/I_G$ ratio, showing the excess of disordered over ideal graphitic domains, decreases with the increasing nitrogen content. The same trend can be observed for the spin concentration (Figure 9).

On the basis of the microscopic and spectroscopic measurements, a simple model of the building unit (a rod) of the CMK-3 material has been developed and is shown in Scheme 2. Its walls resemble a multilayered tube composed of graphene sheets. To satisfy the large fraction of graphene edges (as compared to the layers) shown by the Raman spectra, we postulate that the surface of the rods is not uniform, but it is covered with scale-like flakes exhibiting edges. The core of a rod consists of an amorphous carbon. The built-in N-top nitrogen reduces the number of paramagnetic defects by saturating the dangling bonds

at the edges of the scales. The graphene layers and edges are decorated with surface nitrogen species responsible for the increased polarity of the materials.

Although different in structure, the coaxial pseudospherical layers of the OCM-0.75 replicas exhibit a nonuniform structure of the surface, similar to that of the CMK-3 materials. The apparent difference in the sorption capacities stems from different porosities, although both types of the materials exhibit similar compositions of the nitrogen species.

Conclusions

Two sets of nitrogen-containing carbon materials of hexagonal (CMK-3) and onion-like (OCM-0.75) structures have been obtained via the replication technique with pyrrole as a simultaneous carbon and nitrogen precursor. At the mesoscopic scale, the obtained replicas exhibit well-organized structures built of graphene layers. The extent of their formation is connected with the amount of FeCl_3 at the polymerization stage, showing an optimum with regard to both graphitization degree and nitrogen content. According to the elemental analysis, the total amount of nitrogen incorporated into the studied replicas reaches up to 6.6 wt %, which appears to be a beneficial factor for the sorption properties. The obtained carbons can further be tailored by increasing the concentration of the N-6, N-Q, and N-X species at the expense of the N-5 ones. On the basis of the XPS and EPR results, the structural model showing the way of termination of graphene sheets (being the building layers of the carbons walls) as well as the type and localization of nitrogen groups was proposed.

Acknowledgment. M.L. thanks Dr. Krzysztof Erdmann (Faculty of Chemistry, Nicolaus Copernicus University, Torun, Poland) for help.

References and Notes

- (1) (a) Ozaki, J.; Tanifuji, S.; Kimura, N.; Furuichi, A.; Oya, A. *Carbon* **2006**, *44*, 1324–1326. (b) Meier, M. S.; Andrews, R.; Jacques, D.; Cassity, K. B.; Qian, D. *J. Mater. Chem.* **2008**, *18*, 4143–4145. (c) Miller, D. R.; Wang, J.; Gillan, E. G. *J. Mater. Chem.* **2002**, *8*, 2463–2469. (d) Delgado, J. L.; Herranz, M. A.; Martin, N. *J. Mater. Chem.* **2008**, *18*, 1417–1426.
- (2) Lahaye, J.; Nanse, G.; Bagreev, A.; Strelko, V. *Carbon* **1999**, *37*, 585–590.
- (3) (a) Przeplórski, J. *J. Hazard. Mater.* **2006**, *B135*, 453–456. (b) Szymański, G. S.; Grzybek, T.; Papp, H. *Catal. Today* **2004**, *90*, 51–59. (c) Subramanian, N. P.; Li, X.; Nallathambi, B. N.; Kumaraguru, V.; Colon-Mercado, S. P.; Wu, H.; Lee, G.; Popov, J.-W. *J. Power Sources* **2009**, *188*, 38–44.
- (4) *Chemistry and Physics of Carbon*; Radovic, L. R., Ed.; CRC Press: 2008; Vol. 30, pp 156–159.
- (5) Yang, C.-M.; Weidenthaler, C.; Spliethoff, B.; Mayanna, M.; Schueth, F. *Chem. Mater.* **2005**, *17*, 355–358.
- (6) Fuertes, A. B.; Centeno, T. A. *J. Mater. Chem.* **2005**, *15*, 1079–1083.
- (7) Lee, J.; Jin, S.; Hwan, Y.; Park, J.-G.; Park, H. M.; Hyeon, T. *Carbon* **2005**, *43*, 2536–2543.
- (8) Lezanska, M.; Wloch, J.; Kornatowski, J. *Stud. Surf. Sci. Catal.* **2008**, *174 B*, 945–948.
- (9) Garsuch, A.; Sattler, R. R.; Witt, S.; Klepel, O. *Microporous Mesoporous Mater.* **2006**, *89*, 164–169.
- (10) Xia, Y.; Mokaya, R. *Chem. Mater.* **2005**, *17*, 1553–1560.
- (11) Kawabuchi, Y.; Sotowa, C.; Kishino, M.; Kawano, S.; Whitehurst, D. D.; Moschida, I. *Langmuir* **1997**, *13*, 2314–2317.
- (12) Boudou, J. P.; Chehimi, M.; Broniek, E.; Siemieniewska, T.; Bimer, J. *Carbon* **2003**, *41*, 1999–2007.
- (13) Poole, S. K.; Poole, C. F. *Anal. Commun.* **1997**, *34*, 247–251.
- (14) Szymanski, G. S.; Biniak, S.; Rychlicki, G. *Fuel Process. Technol.* **2002**, *79*, 217–223.
- (15) Lezanska, M.; Wloch, J.; Niedojadlo, J.; Kornatowski, J. *Microporous Mesoporous Mater.* **2008**, *111*, 463–469.
- (16) Dyrek, K.; Rokosz, A.; Madej, A. *Appl. Magn. Reson.* **1994**, *6*, 309–332.

- (17) Jang, J.; Oh, J. H.; Stucky, G. D. *Angew. Chem., Int. Ed.* **2002**, *41*, 1016–1019.
- (18) Han, C.-C.; Lee, J.-T.; Chang, H. *Chem. Mater.* **2001**, *13*, 4180–4186.
- (19) Han, C.-C.; Lee, J.-T.; Yang, R.-W.; Han, C.-H. *Chem. Mater.* **2001**, *13*, 2656–2665.
- (20) Mathys, G. I.; Truong, V.-T. *Synth. Met.* **1997**, *89*, 103–109.
- (21) Mueller, J. O.; Su, D. S.; Wild, U.; Schloegl, R. *Phys. Chem. Chem. Phys.* **2007**, *9*, 4018–4025.
- (22) Nanse, G.; Papirer, E.; Fioux, P.; Moguet, F.; Tressaud, A. *Carbon* **1997**, *35*, 175–194.
- (23) Pels, J. R.; Kaptein, F.; Moulijn, J. A.; Zhu, Q.; Thomas, K. M. *Carbon* **1995**, *33*, 1641–1653.
- (24) Darmstadt, H.; Roy, C.; Kaliaguine, S.; Choi, S. J.; Ryoo, R. *Carbon* **2002**, *40*, 2673–2683.
- (25) Marton, D.; Boyd, K. J.; Al-bayati, A. H.; Tordorov, S. S.; Rabalais, J. W. *Phys. Rev. Lett.* **1994**, *73*, 118–121.
- (26) Sadezky, A.; Muckenhuber, H.; Grothe, H.; Niessner, R.; Pöschl, U. *Carbon* **2005**, *43*, 1731–1742.
- (27) Cuesta, A.; Dhamelincourt, P.; Laureyns, J.; Martinez-Alonso, A.; Tascón, J. M. D. *J. Mater. Chem.* **1998**, *8*, 2875–2879.
- (28) Beyssac, O.; Goffé, B.; Petitem, J. P.; Froigneux, E.; Moreau, M.; Rouzaud, J. N. *Spectrochim. Acta, Part A* **2003**, *59*, 2267–2267.
- (29) Darmstadt, H.; Roy, C. *Carbon* **2003**, *41*, 2662–2665.
- (30) Cuesta, A.; Dhamelincourt, P.; Laureyns, J.; Martinez-Alonso, A.; Tascón, J. M. D. *Carbon* **1994**, *32*, 1523–1532.
- (31) Matsubara, K.; Tsuzuku, T.; Sugihara, K. *Phys. Rev. B* **1991**, *44*, 11845–11851.
- (32) Nakada, K.; Fujita, M.; Dresselhaus, G.; Dresselhaus, M. S. *Phys. Rev. B* **1996**, *54*, 17954–17961.
- (33) Spalek, T.; Pietrzyk, P.; Sojka, Z. *J. Chem. Inf. Model.* **2005**, *45*, 18–29.
- (34) Więckowski, A. B.; Wojtowicz, W.; Pilawa, B. *Fuel* **2000**, *79*, 1137–1141.
- (35) Garaj, V.; Hien-Nga, L.; Gaal, R.; Forro, L.; Takahashi, K.; Kokai, F.; Yudasaka, M.; Iijima, S. *Phys. Rev. B* **2000**, *62*, 17115–17119.
- (36) Blinc, R.; Cevc, P.; Arèon, D.; Zalar, B.; Zorko, A.; Apih, T.; Milia, F.; Madsen, N. R.; Christy, A. G.; Rode, A. V. *Phys. Status Solidi B* **2006**, *13*, 3069–3072.
- (37) Panich, M.; Shames, A. I.; Nakajima, T. *J. Phys. Chem. Solids* **2001**, *62*, 959–964.
- (38) Schmeisser, D.; Bartl, A.; Dunsch, L.; Naarmann, H.; Göpel, W. *Synth. Met.* **1998**, *93*, 43–58.
- (39) Demichelis, F.; Rong, X. F.; Schreiter, S.; Tagliaferro, A.; De Martino, C. *Diamond Relat. Mater.* **1995**, *4*, 361–365.

JP909529X